

Effect of impurity and temperature changes on the thermoelectric properties of the (6, 3) two sided-closed single-walled boron nitride nanotubes ((6, 3) TSC-SWBNNTs)

Ali Mohammad Yadollahi¹, Peyman Azimi Anaraki^{1*}, Mojtaba Yaghobi², Mohammad Reza Niazi²

Abstract

In this study, the thermoelectric properties of the (6, 3) two sided-closed single-walled boron nitride nanotubes are investigated. To examine the effect of the impurity on the thermoelectric properties, carbon atom is replaced instead of boron and nitrogen atoms at the center, left and right the nanotube. The energy range is selected as -5.5 to 5.5 eV and temperatures is considered as 200, 300, 500, 700, 900, 1100 and 1300 K. Investigations show that with increasing temperature and creating impurity, the bandgap of the nanotube significantly reduces. The greatest reduction in the bandgap and the least reduction in the height of the peaks is related to the temperature of 1300 K, in which the carbon atom is replaced instead of nitrogen atom in the center of the nanotube. By increasing temperature, the number of peaks decreases, the mobility of electrons and holes increases and their localization decreases. Also, results show that the largest Seebeck coefficient is related to the temperature of 1300 K and in the case of carbon impurity instead of boron atom at the left side of the nanotube. The magnitude of the maximum of Seebeck coefficient is about $500\mu\text{V/K}$. Besides, the minimum amount of Seebeck coefficient is about $-600\mu\text{V/K}$, which is related to carbon impurity instead of boron at the center of (6.3) TSC-SWBNNT. The largest thermal conductivity is equal to 5.1 nW/K which is related to the pure (6, 3) TSC-SWBNNT at the energy of -4.3 eV . The thermal conductivity values are in the nano (10^{-9}) range, which is small amounts. Studies demonstration that the highest amount of ZT is equal to 1.65 which is related to the impurity of carbon atom instead of boron on the right side of the (6.3) TSC-SWBNNT at the temperature of 1300 K. This value occurs at the energy of -5.2 eV . As the values of ZT are larger than 1, especially at high temperatures, one can conclude that (6, 3) TSC-SWBNNTs is suitable selection as a thermoelectric material.

Keywords

Nanotube, Seebeck coefficient (thermal power), Coefficient of merit, Thermal conductivity, Electrical conductivity.

¹ Department of Physics, Takestan Branch, Islamic Azad University, Takestan, Iran.

² Department of Physics, Ayatollah Amoli Branch, Islamic Azad University, Amol, Iran.

*Corresponding author: peyphysics2004@yahoo.co.uk

1. Introduction

Thermoelectric materials can be considered as sources of clean energy which can be used to convert heat into electricity [1,2]. Thermoelectric materials, using green technologies, can reduce energy crises by converting waste heat into electricity. The thermoelectric performance of the material is evaluated using a dimensionless figure-of-merit, $ZT = S^2 T \sigma / (k_e + k_l)$ where T, S, σ, k_e and k_l are absolute temperature, Seebeck coefficient, electrical conductivity, electronic contribution to thermal conductivity and thermal conductivity of the lattice (phonons), respectively [3,4]. Semiconductors materials can be high efficiency thermoelectric materials. In an organic semiconductor with non-stationary π electrons, the energy gap is an important property among the thermoelectric char-

acteristics of the molecule, which depends on the position of the highest occupied molecular orbital (HOMO), the low unoccupied molecular orbital (LUMO), and the Fermi energy level relative to HOMO and LOMO [1-7].

The Seebeck coefficient is used to investigate and improve the electronic and thermoelectric properties of nanostructures. The values of Seebeck coefficient in semiconductors are from several hundred to several thousand microvolts per Kelvin ($\mu\text{V/K}$) and in metals about a few $\mu\text{V/K}$ [6]. By adding impurities to the structure of a semiconductor, their Seebeck coefficient and the thermoelectric coefficients (which can be positive or negative depending on the type and amount of impurities) can be increased [7].

ZT is a good factor for choosing a structure with suitable

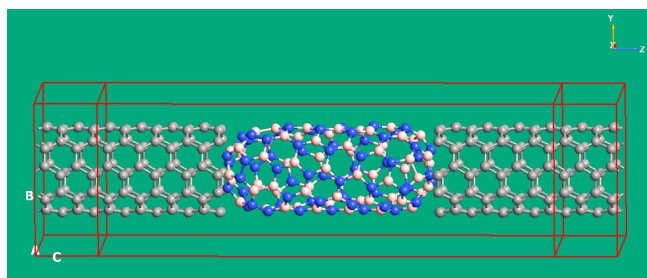


Figure 1. Device made with pure (6, 3) TSC-SWBNNT and two (5, 5) CNT electrode on both sides.

thermoelectric properties. A high-efficiency thermoelectric material has high electrical conductivity, high Seebeck coefficient, low thermal conductivity, and large ZT [8, 9]. In nanostructures, quantum effects improve the value of the Seebeck coefficient and electrical conductivity [10, 11]. Furthermore, by decreasing phonon scattering, the thermal conductance decreases [12, 13].

Nanotubes are among the nanostructures that is anticipated to have suitable thermoelectric properties. The unique electronic, mechanical [14, 15] and thermal properties of carbon nanotubes (CNTs) have led to their widespread applications in transistors, internal connections, and management of the generated heat [16]. To realize the application of the nanotube in the thermoelectric field, their thermal properties should be investigated.

Phonons play a major role in the thermal conductivity of nanotubes. Temperature, defects, impurities, and diameter of CNTs affect the amount and velocity of the phonons. High crystalline order, long average free path length, and high velocity of phonons in nanotubes influence positively on the thermal conductivity [17]. The share of phonons in the heat capacity of CNTs is one hundred times greater than the share of electrons [18]. The average free path length of phonons in nanotubes is estimated in micrometers range. However, this length decreases due to phonon scattering caused by phonon-phonon, phonon-boundary, and phonon-defect interactions [19].

Boron nitride (BN) is a chemically resilient refractory mixture that comprises boron and nitrogen atoms that gives it special characteristics including a notable modulus of elasticity and efficient heat transfer [20]. Since boron nitride nanotubes (BNNT) have better electrical and thermal properties than CNTs, they are a good alternative to CNTs. BNNTs were first predicted in 1994 [21–26], and synthesized experimentally a year later [27]. They have a bandgap of 5–6 eV [21–23]. This bandgap is caused by electronegativity difference between boron and nitrogen, which leads a partial ionic bond between boron and nitrogen. CNTs are resistant to oxidation up to 500°C. However, BNNTs are resistant to oxidation up to 1000°C [28, 29]. BNNTs without defect possess attractive physical properties. However, defects are inevitable. One of the types of defects is the presence of impurities [30–34]. If a carbon atom is placed in a BNNT instead of N or B atom,

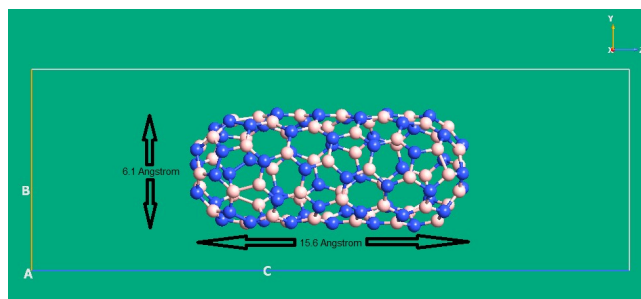


Figure 2. (6, 3) two-sided closed boron nitride nanotube.

the nanotube becomes an n or p type semiconductor, respectively [35, 36].

Due to the wide range of applications of BNNTs, in this study the thermoelectric properties of pure and impure (6, 3) two sided-closed single-walled boron nitride nanotube ((6, 3) TSC-SWBNNTs) are investigated. For this purpose, the nanotube is located between two electrodes made of (5, 5) CNT (see Fig. 1). To examine the effect of the impurity on the thermoelectric properties (electrical conductivity, Seebeck coefficient, thermal conductivity, ZT), carbon atom is replaced instead of boron and nitrogen atoms at the center, left and right the nanotube. The energy range is selected as -5.5 to 5.5 eV and temperatures is considered as 200, 300, 500, 700, 900, 1100 and 1300 K. For this purpose, Slater-Koster [37] and ForceField [38] methods, tight-binding approximation, and non-equilibrium Green's function (NEGF) methods are used. Also, The ATK software is used for the simulations.

Research on boron nitride nanotubes has been done before, but not theoretically on two sided-closed single-walled boron nitride nanotubes, and this is a new study examining the thermoelectric properties of two sided-closed single-walled boron nitride nanotubes are used to convert heat into electrical current, which is used to prevent heat loss. The results of this study can be useful in the design of nanoelectronic and cooling systems.

2. Methodology

According to Fig. 2, the number of N and B atoms in (6, 3) TSC-SWBNNTs is equal to 60 atoms. The diameter of this nanotube is about 6.1 Å and its length is about 15.6 Å. Due to the large number of atoms, the ATK software is used for the simulations.

In this study, Slater-Koster [37] and ForceField [38] methods, tight-binding approximation, and non-equilibrium Green's function (NEGF) methods are used. The chirality of the nanotube is chosen as (6, 3). The two sides of the nanotube are closed using pentagons and hexagons made of boron and nitrogen atoms. The (6, 3) TSC-SWBNNTs is connected to the electrodes via a hexagon made of boron and nitrogen atoms. The plate passing through this hexagon on both sides of the nanotube is located parallel to the cross section of the electrodes.

The axis of the (6, 3) TSC-SWBNNTs is considered parallel

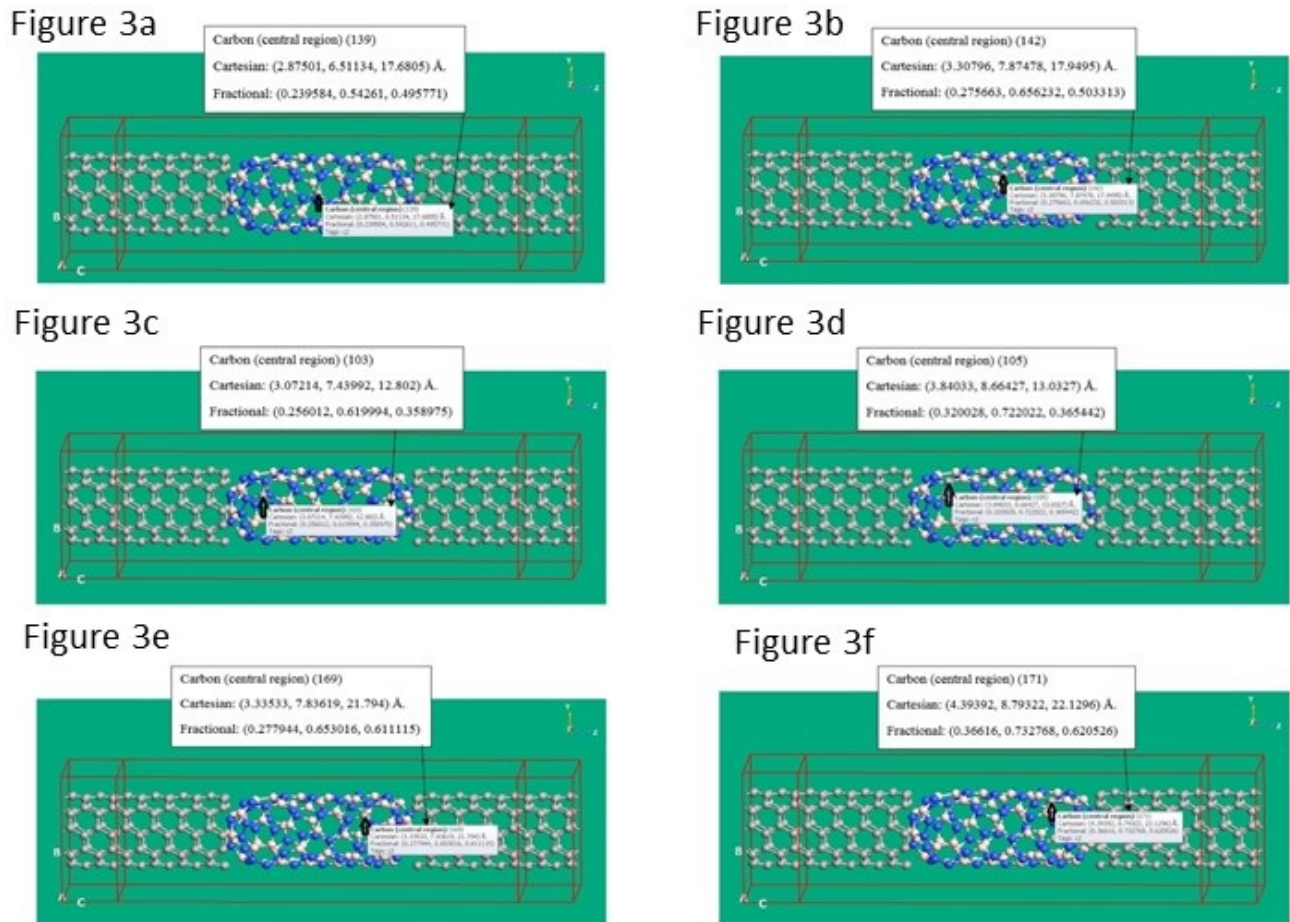


Figure 3. 3-a: Device made of (6, 3) TSC-SWBNT with carbon atom impurity instead of boron atom on the center and two (5, 5) CNT electrodes on both sides. 3-b: Device made of (6, 3) TSC-SWBNT with impurity of carbon atom instead of nitrogen atom on the center and two (5, 5) CNT electrodes on both sides. 3-c: Device made of (6, 3) TSC-SWBNT with carbon atom impurity instead of boron atom on the left and two (5, 5) CNT electrodes on both sides. 3-d: Device made of (6, 3) TSC-SWBNT with carbon atom impurity instead of nitrogen atom on the left and two (5, 5) CNT electrodes on both sides. 3-e: Device made of (6, 3) TSC-SWBNT with carbon atom impurity instead of boron atom on the right and two (5, 5) CNT electrodes on both sides. 3-f: Device made of (6, 3) TSC-SWBNT with carbon atom impurity instead of nitrogen atom on the right and two (5, 5) CNT electrodes on both sides.

to the z-axis. During the simulation method, the mesh cutoff is equal to 150 Rydberg [38, 39]. Brillouin area with K-point, $100 * 1 * 1$ [37, 38] is chosen. To optimize the device, a force tolerance of 0.01 eV/Å with a maximum of 500 steps is used. To obtain thermoelectric properties, energy range of -5.5 to 5.5 eV and bias voltage in the range of 0 to 5 V are employed. (5,5) CNT with $1 * 1 * 4$ repetitions is use in the electrodes. In this study, thermoelectric properties including electrical conductivity, thermal conductivity, Seebeck coefficient, and ZT of the pure and (6,3) TSC-SWBNT are evaluated. For impurity, the B and N atoms are substituted by one carbon atom in the center, left, and right sides of the nanotube (see Figures 3-a to 3-f). The investigations were performed at temperatures of 200, 300, 500, 700, 900, 1100, and 1300 K. According to the NEGF relationship, the transmission func-

tion $T(E, V)$ with energy E and bias voltage V is obtained by the following relation [38–40]:

$$T(E, V) = Tr[\Gamma_L(V)G^R(E, V)\Gamma_R(V)G^A(E, V)] \quad (1)$$

Where G^R and G^A are the retarded and advanced Green's functions of the central scattering region, respectively. $\Gamma_{LR} = i[\Sigma_{L(R)}^R(E) - \Sigma_{L(R)}^A(E)]$ is broadening function, $\Sigma_{L(R)}^R(E)$ and $\Sigma_{L(R)}^A(E)$ are the self-energies of the central scattering region that include all the effects of the electrodes [38–40]. System current is expressed by the Landauer-Buttiker relation [33, 38, 41, 42]:

$$I(V) = \frac{2e}{h} \int [f(E - \mu_L) - f(E - \mu_R)]T(E, V)dE \quad (2)$$

Here h is Planck's constant, e is electron charge, $f(E - \mu_{L(R)})$

Figure 4a

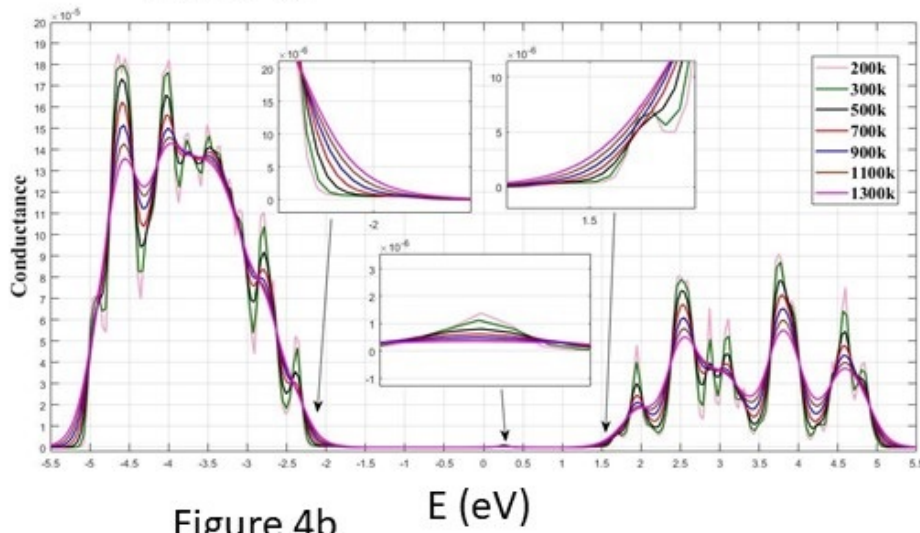


Figure 4b

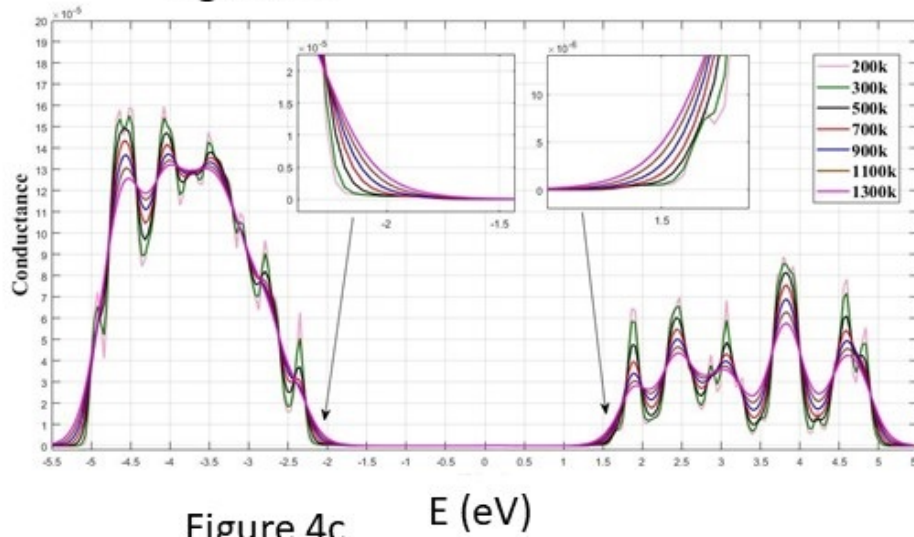


Figure 4c

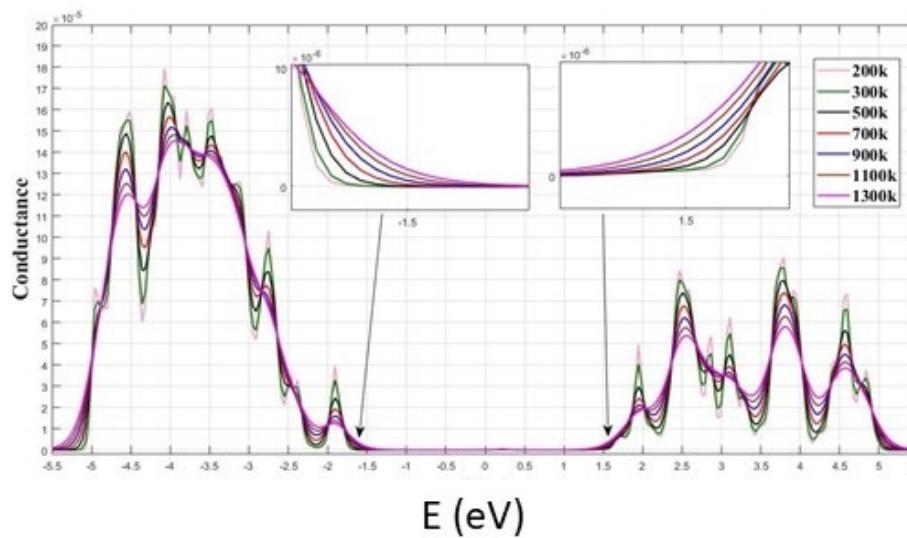


Figure 4d

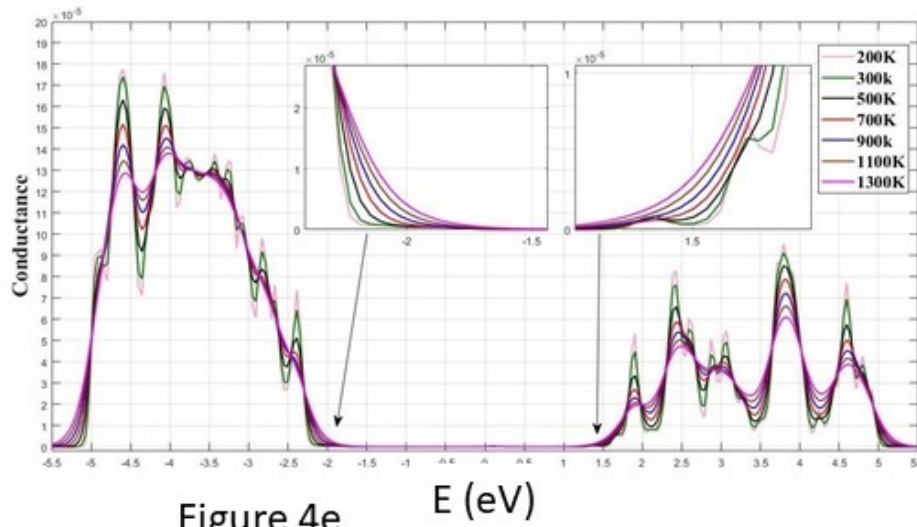


Figure 4e

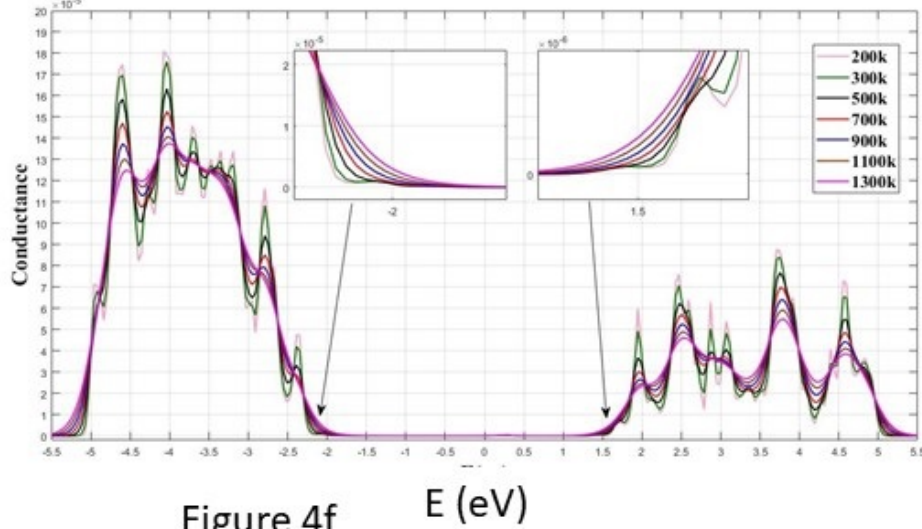
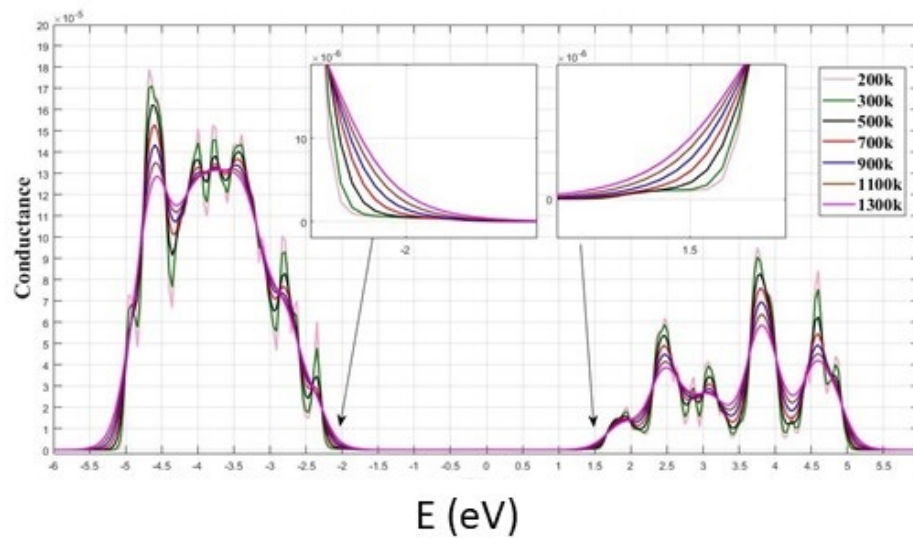


Figure 4f



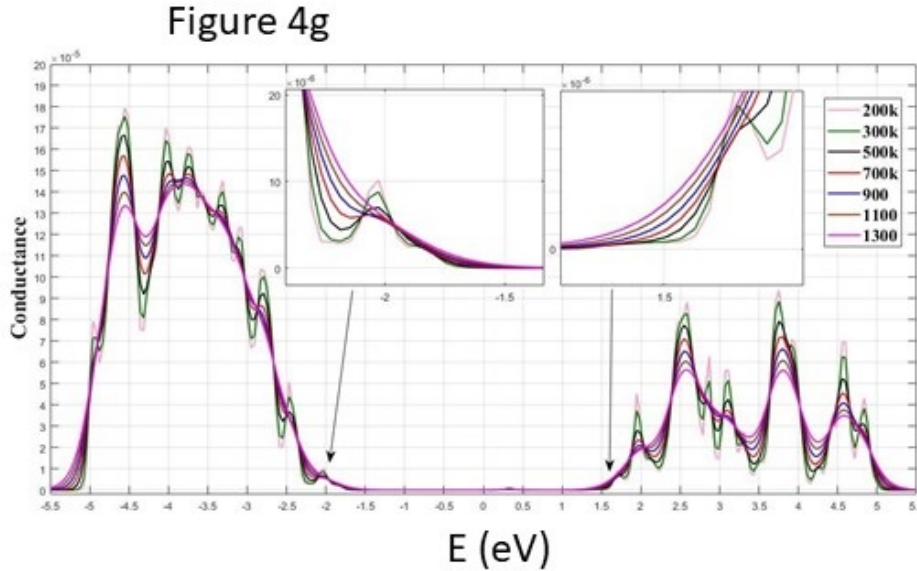


Figure 4. 4-a: Electrical conductivity of (6, 3) TSC-SWBNT at different temperatures a) without impurity b: with carbon impurity instead of boron in the center c) with carbon impurity instead of nitrogen in the center d) with carbon impurity instead of boron on the left e) with carbon impurity instead of nitrogen on the left f) with carbon impurity instead of boron on the right g)with carbon impurity instead of nitrogen on the right.

is function of the Fermi distribution of electrons in the left (right) electrode, and $\mu_{L(R)}$ is the electrochemical potential of the left (right) electrodes [36, 39, 42, 43]. In the linear response region, thermoelectric coefficients are obtained by applying a voltage difference (dV) or temperature difference (dT) between the two electrodes. Electrical conductance (G_e) is obtained from the following equation [43–45]:

$$G_e = \frac{dI}{dV} |_{dT=0} \quad (3)$$

The Peltier coefficient which is used in cooling machines is obtained from the following equation [38–40]:

$$\Pi = \frac{I_Q}{I} |_{dT=0} \quad (4)$$

Seebeck coefficient (thermopower) is expressed as [43–45]:

$$S = -\frac{dV}{dT} |_{I=0} = \frac{\Pi}{V} \quad (5)$$

The thermal conductance equals the sum of the electron thermal conductance and the phonon thermal conductance and is obtained as follows [43–45]:

$$k = k_e + k_{ph} = \frac{dI_Q}{dT} |_{I=0} \quad (6)$$

In the nonlinear reaction regime, the total current flowing and the energy flux are obtained as where I_Q is heat current and calculated from the following equation [43–45]:

$$I_Q = \frac{dQ}{dT} \quad (7)$$

Electrons conventional thermal conductance at zero electron current, is given through the following expressions [46]:

$$k = \left(-\frac{I_Q}{\Delta T}\right)_{I_e=0} = e \left[-SL_1 + \frac{k_B}{e} \beta_R L_2\right] \quad (8)$$

Additionally, one can calculate the Seebeck S as [46]:

$$S = \left(-\frac{\Delta V}{\Delta T}\right)_{I_e=0} = \frac{k_B \beta_R L_1}{e L_0} \quad (9)$$

The coefficients L_n ($n = 0, 1$ and 2) are defined as [46, 47]:

$$L_n = \frac{2}{h} \int_{-\infty}^{\infty} \sum_{m,n} [-\epsilon]^n \left(-\frac{\partial f}{\partial \epsilon}\right) P_m T_{m,n}(\epsilon) d\epsilon \quad (10)$$

In the nonlinear reaction regime, the total current flowing and the energy flux are obtained as [46, 48]:

$$I_e(V_b) = \frac{2e}{h} \int_{-\infty}^{\infty} \sum_{m,n} [P_m f_L^m (1 - f_R^n) - P_n f_L^n (1 - f_R^m)] T_{m,n}(\epsilon, V_b) d\epsilon \quad (11)$$

$$I_Q(V_b) = \frac{2}{h} \int_{-\infty}^{\infty} \sum_{m,n} [P_m f_L^m (1 - f_R^n) - P_n f_L^n (1 - f_R^m)] T_{m,n}(\epsilon, V_b) d\epsilon \quad (12)$$

Here $f_\alpha^m(\epsilon, V_b) = \exp[\beta_\alpha(\epsilon + mh\omega - \mu_\alpha)] + 1$ is the Fermi-Dirac distribution function, $P_m = [1 - \exp(\beta_R h\omega)] \exp(\beta_R mh\omega)$ is the Boltzmann distribution function, $\mu_{L,R} = E_f \pm 1/2eV_b$

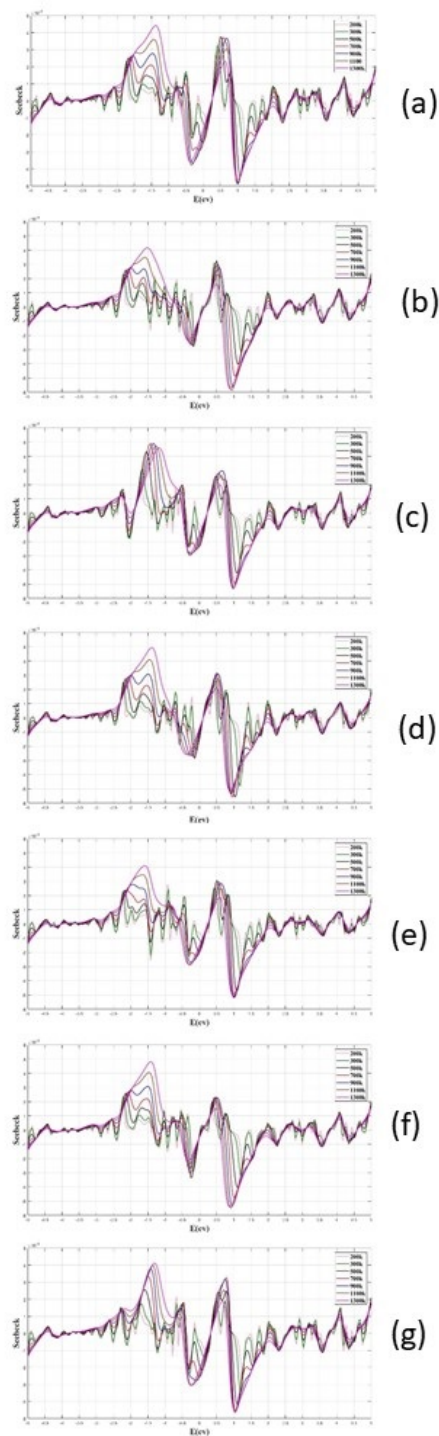


Figure 5. Seebeck coefficient (thermopower) of (6, 3) TSC-SWBNT at different temperatures a) without impurity b) with carbon impurity instead of boron in the center c) with carbon impurity instead of nitrogen in the center d) with carbon impurity instead of boron on the left e) with carbon impurity instead of nitrogen on the left f) with carbon impurity instead of boron on the right g) with carbon impurity instead of nitrogen on the right.

is used to represent the electrochemical potential of the electrodes located on the left and right, respectively, e is the electron charge and h is the Planck's constant.

In the linear response area, the thermoelectric factors are presented by the following expressions: [46, 49]

$$\begin{pmatrix} I_e \\ I_Q \end{pmatrix} = \begin{pmatrix} e^2 L_0 & ek_B \beta_R L_1 \\ e L_1 & k_B \beta_R L_2 \end{pmatrix} \begin{pmatrix} V \\ \delta \theta \end{pmatrix} \quad (13)$$

These expressions indicate that the energy and charge fluxes are straightly dependent on the difference between the chemical potential $V = (\mu_L - \mu_R)/e$ and the temperature difference $\Delta \theta = \theta_L - \theta_R$.

The incoming channel m with the outgoing channel n are connected based on transmission probability of individual transitions [46].

$$T_{m,n}(\varepsilon, V_b) = \text{tr}[\hat{\Gamma}_L \hat{G}_{m+1,n+1}^R \hat{\Gamma}_R \hat{G}_{m+1,n+1}^A] \quad (14)$$

The transmission function depends on the energy and the bias voltage. Here, the coupling function $\Gamma_{L,R}$ is the line widths function, and G_C^R is the advanced and retarded Green's function of the left and right electrodes, respectively. In addition, electron energies are confined by the energy conservation law $\varepsilon_{in} + mh\omega = \varepsilon_{out} + nh\omega$. It should be noted that the elastic contributions can be achieved by imposing the finiteness of elastic transitions where $\varepsilon_{in} = \varepsilon_{out}$ or more accurately $m = n$. By applying the bias voltage, the Green's function of the structure is appraised from the effective Hamiltonian of the molecule (H_c) and self-energy functions (Σ) as [46, 50, 51]:

$$G_{\alpha}^R(\varepsilon, V_b) = [(\varepsilon \pm i\eta)\hat{I} - H_C - \sum_L(\varepsilon, V_b) - \sum_R(\varepsilon, V_b)]^{-1} \quad (15)$$

here $\eta = 0^+$ is a positive infinitesimal constant. Using the wide band approximation, the self-energy matrices of the left and right leads are determined as [46, 50-51]:

$$\Sigma_{\alpha} = 2i\Gamma_{\alpha} = -\hat{\tau}_{\alpha C}^{\dagger} \hat{g}_{\alpha} \hat{\tau}_{\alpha C} \quad (\alpha = L, R) \quad (16)$$

Where $\hat{\tau}$ is the hopping matrix coupling the molecule to the leads, and its elements is the independent of the energy. $\hat{g}_{\alpha} = i\pi\rho_{\alpha}$ is the surface Green's function of the uncoupled α -electrode, and ρ_{α} is the density of states of the α -electrode for the Fermi energy.

The dimensionless thermoelectric coefficient (ZT) is obtained from the following equation [43–45]:

$$ZT + \frac{G_e S^2 T}{k} \quad (17)$$

The above relations show how applying a temperature difference leads to a voltage difference in a thermoelectric material. These coefficients in the linear response area are calculated by the Thermoelectric Coefficients plugin in ATK software.

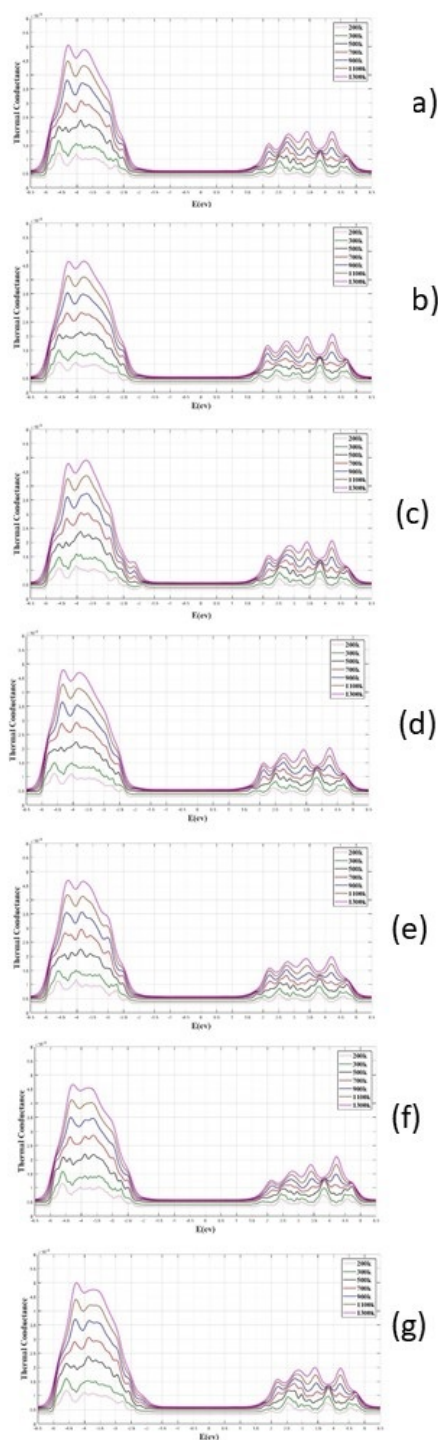


Figure 6. Thermal conductivity of (6, 3) TSC-SWBNT at different temperatures a) without impurity b) with carbon impurity instead of boron in the center c) with carbon impurity instead of nitrogen in the center d) with carbon impurity instead of boron on the left e) with carbon impurity instead of nitrogen on the left f) with carbon impurity instead of boron on the right g) with carbon impurity instead of nitrogen on the right.

3. Results and discussion

In this study, thermoelectric properties of (6.3) TSC-SWBNT, including electrical conductance, Seebeck coefficient, thermal conductance and merit coefficient (ZT), are investigated. Larger merit coefficient of material indicates that it is a better thermoelectric substance. This coefficient increases by increasing temperature, electrical conductivity and Seebeck coefficient and decreasing thermal conductivity. The mentioned thermoelectric properties are computed for pure (6, 3) TSC-SWBNTs and impure nanotube by applying carbon impurity instead of boron and nitrogen atoms at three locations including center, left, and right side of this nanotube. Moreover, the simulations are performed at different temperatures in the range of 200 to 1300 K.

Figures of 4-a to 4-g indicate the electrical conductivity of (6.3) TSC-SWBNT with carbon impurity instead of boron and nitrogen. In figures, electrical conductivities are drawn at different temperatures. Some similar results are observed in all figures. In all diagrams, the left half of the curves is higher than the right half of it, which indicates larger density of charge carriers in the capacity band and the high impact of capacity band on electrical conductivity. In all of these figures, the height of the peak reduces by increasing the temperature, and instead, electrons and holes move towards HOMO (the highest occupied molecular orbital) and LUMO (the low unoccupied molecular orbital). Hence, the bandgap reduces and the electrical conductivity increases.

Besides, by increasing temperature, the number of excited phonons increases which prevents more transmission of charge carriers. This results in reducing the electrical conductivity. Moreover, by increasing temperature, the number of peaks decreases. Therefore, it can be concluded that by increasing temperature, the mobility of electrons and holes increases and their localization decreases. On the other hand, the bandgap decreases by increasing the temperature. The highest decrease is observed at the temperature of 1300 K. The bandgap of the impure nanotube is significantly smaller than that of pure nanotubes. This decrease depends on the atom instead of which the C atom is replaced. Considering that the carbon atom has one more electron than boron atom, substituting C atom instead of B atom nanotube is converted to n-type semiconductor [29,52,53]. In this case, the bandgap significantly reduces from the right, which can be seen in Figures of 4-b, 4-d and 4-f.

By replacing the carbon atom instead of nitrogen atom, considering that the carbon atom has an electron less than nitrogen atom, the (6.3) TSC-SWBNT is converted into p-type semiconductor [29,52,53]. In this case, the bandgap is significantly reduced from the left side of the curves which can be seen in Figures of 4-c, 4-e and 4-f. The greatest reduction in the bandgap and the least reduction in the height of the peaks is related to Figure 4-C and the temperature of 1300 K, in which the carbon atom is replaced instead of nitrogen atom in the center of the nanotube. As it was previously mentioned, replacement of carbon atom instead of nitrogen atom converts

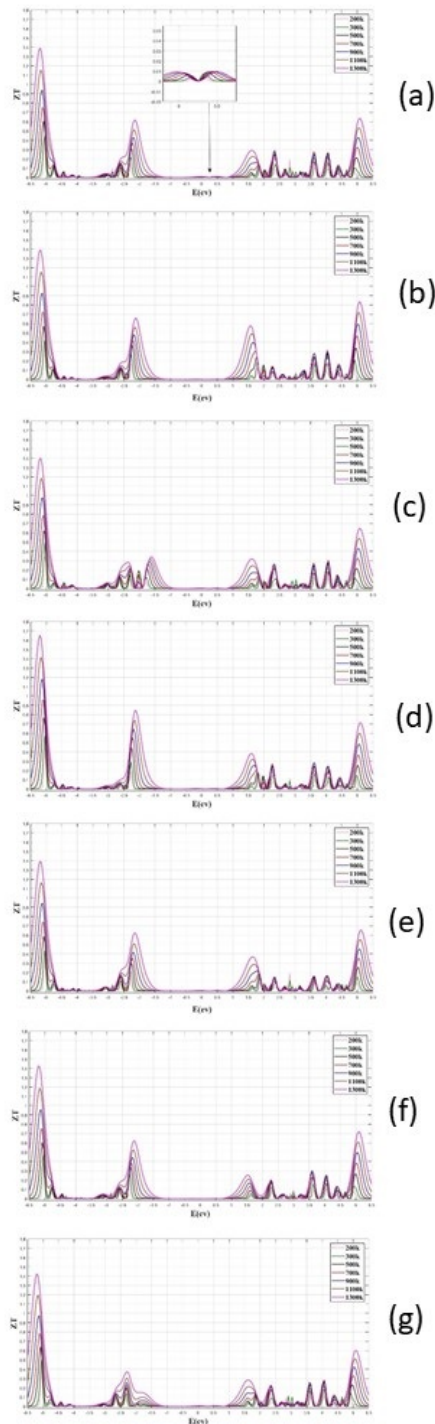


Figure 7. Merit coefficient (ZT) of (6, 3) TSC-SWBNNT at different temperatures a) without impurity b) with carbon impurity instead of boron in the center c) with carbon impurity instead of nitrogen in the center d) with carbon impurity instead of boron on the left e) with carbon impurity instead of nitrogen on the left f) with carbon impurity instead of boron on the right g) with carbon impurity instead of nitrogen on the right.

the nanotube into a p-type semiconductor. Due to the higher density of electrons and holes at the two ends of the nanotube and near the boundaries and their lower density in the center, the effect of this impurity in the center is more observable than the impurity on the left and right side.

Figures of 5-a to 5-g represent the Seebeck coefficient for different conditions of carbon impurity instead of boron and nitrogen in the center, left and right side of the (6,3) TSC-SWBNNT. The effect of the temperature on the Seebeck coefficient can be studied in these figures. By increasing the temperature, the number of peaks in diagrams of the Seebeck coefficient reduces. This can be related to increasing the mobility of electrons and holes and decreasing their localization by increasing the temperature. The largest changes in the Seebeck coefficient are in the range of bandgap.

The height of the peaks increases by increasing the temperature, which indicates increase in the Seebeck coefficient. The highest height of the peaks is related to the temperature of 1300 K in the range of -1 to -1.5 eV in each of the figures of 5-a to 5-g. The largest Seebeck coefficient in these figures is related to the temperature of 1300 K and in the case of carbon impurity instead of boron atom at the left side of the nanotube. The magnitude of the maximum of Seebeck coefficient is about $500 \mu\text{V/K}$. Besides, the minimum amount of Seebeck coefficient is about $-600 \mu\text{V/K}$, which is related to carbon impurity instead of boron at the center of (6,3) TSC-SWBNNT. Figures of 6-a to 6-g show thermal conductivity (6, 3) TSC-SWBNNTs in which carbon impurity is located instead of nitrogen and boron in the center, left and right side of the nanotube. Again, the investigations are performed at different temperatures. It can be observed that by increasing the temperature, the height of the peaks increases, that indicate an increase in the thermal conductivity of the nanotube by increasing the temperature. In all diagrams, the left half of the curves is longer than its right half, which represents the density of charge carriers in the capacity band and the high impact of capacity band on thermal conductivity.

According to these figures, the thermal conductivity values are in the nano (10^{-9}) range, which is small amounts. Besides, as it can be seen in Eq. (17), since the thermal conductivity is in the denominator of the equation, for the small values of thermal conductivity larger values of ZT would be obtained. Due to the presence of phonon, the curves of Figures 6-a to 6-g have shifted slightly upwards. Hence, the minimum of thermal conductivity in the range of 0.5 nW/K. In this range, the lowest value is related to the temperature of 200 K, which is lower than 0.5 nW/K and the highest value is associated with the temperature of 1300 K, which is larger than 0.5 nW/K. The largest thermal conductivity is equal to 5.1 nW/K which is related to the pure (6,3) TSC-SWBNNT at the energy of -4.3 eV (see Figure (6-a)). It can also be seen from Figures 6-a to 6-g that the bandgap decreases significantly by increasing the temperature. The increasing intensity depends on the type of semiconductor than nanotube converted into it by replacing the C atom instead of boron (n-type semiconductor) or nitro-

gen (p- type semiconductor).

According Eq. 17, the temperature values, the Seebeck coefficient, and electrical and thermal conductivity affect the value of the ZT . The effects of these parameters on ZT are shown in Figures 7-a to 7-g. Again, the pure and impure (6,3) TSC-SWBNNT investigated. The carbon atom is used as the impurity to be replaced instead of B and N atom at the center, left and right-hand side of the nanotube. The results are reported at different temperatures. It is observed that by increasing the temperature ZT increases. Hence, the highest values of ZT are related to 1300 K. Moreover, by increasing the temperature, the number of peaks decreases which can be related to due to the more mobility and less localization of electrons and holes at larger temperatures. Besides, by increasing the temperature, the length of the bandgap also decreases. The highest amount of ZT is equal to 1.65 which is related to the impurity of carbon atom instead of boron on the right side of the (6,3) TSC-SWBNNT at the temperature of 1300 K (see Fig. 7-d). This value occurs at the energy of 5.2 eV. As the values of ZT are larger than 1, especially at high temperatures, one can conclude that (6, 3) TSC-SWBNNTs is suitable selection as a thermoelectric material.

4. Conclusion

In this study, the thermoelectric properties of pure and impure (6, 3) TSC-SWBNNT were investigated. The C atom was used as the impurity which was replaced instead of boron and nitrogen atoms at three locations of the nanotube including in the center, left, and right of the side. The energy range was considered as -5.5 to 5.5 eV. Besides, all of the simulations were repeated at different temperatures including 200, 300, 500, 700, 900, 1100 and 1300 K.

The general results in this research are as follows:

The results show that by increasing temperature and creating impurity, the bandgap of the nanotube significantly reduces. The greatest reduction in the bandgap and the least reduction in the height of the peaks is related to the temperature of 1300 K, in which the carbon atom is replaced instead of nitrogen atom in the center of the nanotube.

Comparison of electrical conductivity properties shows that with increasing temperature, the number of peaks decreases. Therefore, it can be concluded that by increasing temperature, the mobility of electrons and holes increases and their localization decreases.

The largest Seebeck coefficient is related to the temperature of 1300 K and in the case of carbon impurity instead of boron atom at the left side of the nanotube. The magnitude of the maximum of Seebeck coefficient is about 500 $\mu\text{V/K}$. Besides, the minimum amount of Seebeck coefficient is about -600 $\mu\text{V/K}$, which is related to carbon impurity instead of boron at the center of (6,3) TSC-SWBNNT.

The largest thermal conductivity is equal to 5.1 nW/K which is related to the pure (6, 3) TSC-SWBNNT at the energy of -4.3 eV. In addition, the thermal conductivity values are in the nano (10- 9) range, which is small amounts.

The highest amount of ZT is equal to 1.65 which is related to the impurity of carbon atom instead of boron on the right side of the (6,3) TSC-SWBNNT at the temperature of 1300 K. This value occurs at the energy of -5.2 eV. As the values of ZT are larger than 1, especially at high temperatures, one can conclude that (6, 3) TSC-SWBNNTs is suitable selection as a thermoelectric material.

Conflict of interest statement:

The authors declare that they have no conflict of interest.

References

- [1] F. R. Nikmaram and M. Gholizadeh Arashti. *Journal of Research on Many-body Systems*, **10**:135, 2020.
- [2] M. Zare, J. Abadi, H. Ramin, and R. Hoseini Abardeh. *AmirKabir Journal of Mechanical Engineering*, **45**:83, 2013.
- [3] M. Shojaei, A. Shokuhfar, A. Zolriasatein, and A. O. Moghaddam. *Advanced Powder Technology*, **33**:103445, 2022.
- [4] P. R. Saffari, M. Fakhraie, and M. A. Roudbari. *Micro and Nano Letters*, **15**:181, 2020.
- [5] D. Nozaki, H. Sevencli, W. Li, R. Gutierrez, and G. Cuniberti. *Physical Review B*, **81**:235406, 2010.
- [6] L. Wang, C. Pan, A. Lianga, X. Zhou, W. Zhou, and T. Wan. *Polymer Chemistry*, **8**:4644, 2017.
- [7] M. Salim, S. H. Sharifi, and S. J. Hashemifar. *Iranian Journal of Physics Research*, **15**:97, 2015.
- [8] A. F. Ioffe, L.S. Stilbans, E. K. Jordanishvili, T. S. Stavitskaya, and A. Gelbtuch. *Physics Today*, **12**:42, 1959.
- [9] S. Shimizu, J. Shiogai, N. Takemori, S. Sakai, H. Ikeda, R. Arita, T. Nojima, A. Tsukazaki, and Y. Iwasa. *Nature Communications*, **10**:825, 2019.
- [10] L. D. Hicks and M. S. Dresselhaus. *Physical Review B*, **47**:16631, 1993.
- [11] R. Venkatasubramanian, E. Siivola, T. Colpitts, and B. Quinn. *Nature*, **413**:597, 2001.
- [12] D. Vashae and A. Shakouri. *Journal of Applied Physics*, **95**:1233, 2004.
- [13] G. Zeng, X. Fan, C. Labounty, E. Croke, Y. Zhang, J. Christofferson, D. Vashae, A. Shakouri, and J. E. Bowlers. *MRS Online Proceedings Library (OPL)*, **793**:43, 2003.
- [14] A. Ebrahimi-Mamaghani, A. Forooghi, H. Sarparast, A. Alibeigloo, and M. I. Friswell. *Applied Mathematical Modelling*, **90**:131, 2021.
- [15] A. Ebrahimi-Mamaghani, N. Mostoufi, R. Sotudeh-Gharebagh, and R. Zarghami. *Ocean Engineering*, **249**:110917, 2022.

- [16] A. M. Marconnet, M. A. Panzer, and K. E. Goodson. *Reviews of Modern Physics*, **85**:1296, 2013.
- [17] M. S. Dresselhaus, G. Dresselhaus, and A. Jorio. *Annual Review of Materials Research*, **34**:247, 2004.
- [18] L. X. Benedict, S. G. Louie, and M. L. Cohen. *Solid State Communications*, **100**:177, 1996.
- [19] Z. Wang, D. Tang, X. Zheng, W. Zhang, and Y. Zhu. *Nanotechnology*, **18**:475714, 2007.
- [20] Y. Zarabimanesh, P. Roodgar Saffari, P. Roudgar Saffari, and N. Refahati. *Journal of Vibration and Control*, **28**:2101, 2021.
- [21] X. Blase, A. Rubio, S. J. Louie, and M. L. Cohen. *Europhysics Letters*, **28**:335, 1994.
- [22] A. Rubio, J. L. Corkill, and M. L. Cohen. *Physical Review B*, **49**:5081, 1994.
- [23] C. H. Lee, M. Xie, V. Kayastha, J. Wang, and Y. K. Yap. *Chemistry of Materials*, **22**:1782, 2010.
- [24] M. L. Cohen and A. Zettl. *Physics Today*, **63**:34, 2010.
- [25] A. L. Tiano, C. Park, J. W. Lee, H. H. Luong, L. J. Gibbons, S. H. Chu, S. Applin, P. Gnoffo, S. Lowther, H. J. Kim, P. M. Danehy, J. A. Lnmann, S. B. Jones, J. H. Kang, G. Sauti, S. A. Thibeault, V. Yamakov, K. E. Wise J. Su, and C. C. Fay. *Current Applied Physics*, **9060**:906006, 2014.
- [26] C. H. Lee, S. Bhandari, B. Tiwari, N. Yapici, D. Zhang, and Y. K. Yap. *Molecules*, **21**:922, 2016.
- [27] N. G. Chopra, R. J. Luyken, K. Cherrey, V. H. Crespi, M. L. Cohen, S. G. Louie, and A. Zettl. *Science*, **269**:966, 1995.
- [28] M. Yaghobi, A. Bahari, and M. Yaghobi. *Molecular Physics*, **117**:260, 2019.
- [29] J. X. Zhao and B. Q. Dai. *Materials Chemistry and Physics*, **88**:244, 2004.
- [30] E. Almahmoud and J. A. Talla. *Materials Research Express*, **6**:105038, 2019.
- [31] I. Petrushenko and K. Petrushenko. *Computational Materials Science*, **128**:243, 2016.
- [32] J. F. Jia, H. S. Wu, and H. Jiao. *Physica B: Condensed Matter*, **381**:90, 2006.
- [33] J. X. Zhao, Y. Tian, and B. Q. Dai. *Journal of the Chinese Chemical Society*, **52**:395, 2005.
- [34] J. A. Talla, S. Ayman, and H. Sabbah. *Journal of Computational and Theoretical Nanoscience*, **11**:1838, 2014.
- [35] L. Ci, L. Song, C. Jin, D. Jariwala, D. Wu, Y. Li, A. Srivastava, Z. F. Wang, K. Storr, L. Balicas, F. Liu, and P. M. Ajayan. *Nature materials*, **9**:430, 2010.
- [36] D. A. Papaconstantopoulos and M. J. Mehl. *Journal of Physics: Condensed Matter*, **15**:R413, 2003.
- [37] J. Schneider, J. Hamaekers, S. T. Chill, S. Smidstrup, J. Bulin, R. Thesen, A. Blom, and K. Stokbro. *Modelling and Simulation in Materials Science and Engineering*, **25**:085007, 2017.
- [38] P. Zhao, D. S. Liu, S. J. Li, and G. Chen. *Solid State Communications*, **152**:2040, 2012.
- [39] M. Wang, X. Jiang, X. Li, D. Li, B. Cui, and D. Liu. *Physics Letters A*, **383**:2217, 2019.
- [40] S. Datta. *Electronic transport in mesoscopic systems*. Cambridge University Press, New York, 1th edition, 1995.
- [41] P. Chaudhuri, C. N. Lima, H. O. Frota, and A. Ghosh. *Applied Surface Science*, **536**:147686, 2020.
- [42] C. Rui, C. Shao, J. Liu, A. Chen, K. Zhu, and S. Shao. *Materials Science in Semiconductance Processing*, **130**:105826, 2021.
- [43] H. Alama and S. Ramakrishna. *Nano Energy*, **2**:190, 2012.
- [44] T. A. Luu. *Thermoelectric Materials: Principles, Structure, Properties, and Applications*. Elsevier, 1th edition, 2002.
- [45] T. Markussen, A. P. Jauho, and M. Brandbyge. *Physical Review Letters*, **103**:055502, 2009.
- [46] A. M. Yadollahi, P. Azimi Anaraki, and M. Yaghobi. *Indian Journal of Physics*, **82**, 2022.
- [47] X. Zheng, W. Lu, T. A. Abteu, V. Meunier, and J. Bernholc. *ACS Nano*, **4**:7205, 2010.
- [48] G. D. Guttman, E. Ben-jacob, and D. J. Bargman. *Physical Review B*, **51**:17758, 1995.
- [49] P. Zhao, D. S. Liu, Y. Zhang, Y. Su, S. J. Li, and G. Che. *Physics Letters A*, **375**:2639, 2011.
- [50] L. Wang, K. Tagami, and M. Tsukada. *Japanese Journal of Applied Physics*, **43**:2779, 2004.
- [51] M. R. Niazian, L. F. Matin, M. Yaghobi, and A. A. Masoudi. *Indian Journal of Physics*, **95**:1131, 2021.
- [52] M. R. Roknabadi, M. Ghodrati, M. Modarresi, and F. Koohjani. *Physica B*, **410**:212, 2013.
- [53] R. Sadegh, M. R. Niazian, M. Yaghobi, and M.A. Ramzanpour. *Int. J. Nano Dimens.*, **13**:311, 2022.